INSTITUT DE FRANCE
Académie des sciences

Comptes Rendus

Mécanique

Nguyen Thi Giang and Doan Lan Phuong

New finite modelling of the nonlinear static bending analysis of piezoelectric FG sandwich plates resting on nonlinear elastic foundations

Volume 350 (2022), p. 99-119

Published online: 7 April 2022

https://doi.org/10.5802/crmeca.106

Les Comptes Rendus. Mécanique *sont membres du Centre Mersenne pour l'édition scientifique ouverte*
www.centre-mersenne.org
e-ISSN : 1873-7234

Comptes Rendus
Mécanique
2022, 350, p. 99-119
https://doi.org/10.5802/crmeca.106

Synthesis / *Synthèse*

New finite modelling of the nonlinear static bending analysis of piezoelectric FG sandwich plates resting on nonlinear elastic foundations

Nguyen Thi Giang [*, a] **and Doan Lan Phuong** [a]

[a] University of Transport Technology, 54 Trieu Khuc, Thanh Xuan, Hanoi, Vietnam
E-mails: giangnt@utt.edu.vn (N. T. Giang), phuongdl@utt.edu.vn (D. L. Phuong)

Abstract. This paper presents a new finite modelling of the nonlinear static bending analysis of piezoelectric functionally graded (FG) sandwich plates resting on nonlinear elastic foundations. Finite element formulations are derived by using the first-order shear deformation theory (FSDT) of Mindlin and the finite element method. The proposed theory and mathematical model of this work are verified by comparing the results with those of other methods, and they are in good agreement. A parameter study is conducted to investigate the effects of geometrical and physical properties such as nonlinear factors, volume fraction index, nonlinear foundation parameters, applied voltages, boundary conditions, etc., on the nonlinear mechanical behaviors of piezoelectric FG sandwich plates. The novel numerical results of this work are very important, and can be used as a good reference to examine related structures as well as of use in engineering practice.

Keywords. Nonlinear static bending, Piezoelectric FGM sandwich plate, Third-order shear deformation theory, Nonlinear elastic foundation, Finite element.

Manuscript received 22nd September 2021, revised 2nd March 2022, accepted 15th March 2022.

1. Introduction

Normally, complicated smart structures tend to be formed based on some kinds of materials such as functionally graded materials (FGM), piezoelectric, piezoelectric and electrostrictive ceramics, shape memory alloys and polymers, conductive polymers, and so on. This is to take advantage of the different types of materials and increase the working tolerance of these structures. To investigate the mechanical behaviors of these structures, we need to use more advanced plate theories and it is time intensive to calculate and examine. In order to establish the reasons for carrying out this work, this section first sums up the findings in closely related papers and investigations.

Numerous studies on the mechanical response of multilayer plate structures [1–11] and on elastic foundations [12–17] have been published. For piezoelectric sandwich FGM structures, Moita *et al.* [1] carried out the vibration analysis of an active–passive damped multilayer sandwich structure with a viscoelastic core, sandwiched between FGM layers, where piezoelectric

* Corresponding author.

layers were also attached. In their work, the displacement field of FGM and the piezoelectric layers were modeled by using the classical plate theory, and the core was described by using Reddy's third-order shear deformation theory (TSDT), respectively. Saffari and his co-workers [2] used the TSDT to numerically investigate the free vibration behaviors of three-layered annular FGMs plates subjected to initial external electric voltage. In this study, the impressive material specifications of FGM were assumed to change gradually along the thickness direction of the plate as a power-law distribution. In addition, Newmark-β and Hamilton's methods were employed to solve, by applying the differential quadrature method (DQM). Loja and colleagues [3] studied the static and free vibration behaviors of FG sandwich plate-type structures by using B-spline finite strip element models based on different shear deformation theories, and the effective properties of FGM were estimated according to Mori–Tanaka homogenization scheme. Rasool *et al.* [4] investigated the damped dynamic deflections of an advanced piezoelectric sandwich plate (APSP) under thermo-electro-mechanical loads by using a meshless method. In the proposed mathematical model, two active piezoelectric layers were attached to the surfaces of a passive advanced structure containing two thin graphene reinforced nanocomposite (GRNC) layers and a thick porous polymeric core. Alibeigloo [5] studied the transient response of a simply supported FGM rectangular plate embedded in sensor and actuator piezoelectric layers subjected to both applied electric field and thermal shock based on the theory of piezoelectricity and generalized coupled thermoelasticity. In this, the thermoelastic properties of the plate varied gradually along the plate thickness direction according to exponential functions, and the Poisson's ratio was assumed to have not changed; the Fourier series and Laplace transform were used to solving analytically the basic coupled thermoelastic differential equations. Zenkour *et al.* [6] investigated the static bending of sandwich FGM plate with the faces made of piezoelectric materials under hygro-thermo-electro-mechanical sinusoidal loadings. The displacement fields were expressed by using a two-variable shear deformation plate theory. A series of parameter studies were conducted to evaluate the influences of applied voltage, material anisotropy, side-to-thickness ratio, aspect ratio, thermal expansion coefficients, moisture concentration coefficients, and inhomogeneity parameter on the static behavior of the structure. Gorge *et al.* [7] introduced a finite element model based on a layer-wise model of first-order shear deformation theory (FSDT) to investigate the free vibration responses of axisymmetric piezoelectric shells. Kapuria and Kulkarni [8] presented a five-node element for the mechanical investigation of plates with piezoelectric sensor and actuator layers. The element was based on an ameliorated zig-zag theory for dynamic analysis of the piezoelectric plates. Beheshti-Aval and Lezgy-Nazargah [9] developed a three-node quadratic element without using any shear locking corrections for piezoelectric sandwich plates. Their work used the higher-order global–local theory, where in-plane displacements were presented using a higher-order term, an exponential term, and a term containing first-order derivatives of the electric degrees of freedom (DOF). Plagianakos and Papadopoulos [10] introduced an element by using a higher-order layer-wise theory with a focus on investigating the delamination phenomenon among layers of piezoelectric plates.

For piezoelectric FGM structures resting on elastic foundations, Zenkour *et al.* [12] carried out the static bending analysis of a sandwich plate made of a FG core and face sheets fabricated of piezoelectric material, where the sandwich plate was resting on Pasternak's elastic foundations and subjected to sinusoidal thermo-electro-mechanical loads. The equilibrium equations were constructed using the virtual work principle and solved by Navier's solution approach. Mohammadimehr and his co-workers [13] employed the TSDT and the Navier's type solution to analytically investigate the free vibration and buckling of a piezoelectric FGM sandwich plate resting on the Pasternak foundation subjected to normal pressure. Abazid *et al.* [14] examined the static bending of some types of FGM sandwich plates resting on the Pasternak's two-parameter elastic foundations in a hygrothermal environment. From the above-mentioned works, one can see

that there are no publications relating to mechanical responses of sandwich FGM plates resting on elastic foundations taking into account the effect of the nonlinearity, which was proposed by Babaei *et al.* [15].

In practice, sandwich structures may rest on other elastic bodies, where in some cases, they can be considered as elastic foundations. In the case of mechanical behaviors of an elastic foundation changing nonlinearly according to the displacement field of the plate, mechanical response in this nonlinear case is much different from that of the linear one. This is an important and interesting point, which has not been considered in other publications. Besides, during the working process, large deformations can occur in structures, therefore, nonlinear investigations of these structures need to be conducted, especially, for the structures resting on nonlinear elastic foundations. Additionally, scientists have employed multi-layer structures to boost the efficiency of using structures constructed of FGM materials. This is a multi-layer construction that maximizes the benefits of both ceramic and metal structures while also enhancing their ultimate strength. For the above reviews, as can be seen, examining the nonlinear response of multilayer sheets constructed of FGM materials with piezoelectric layers and mounted on a nonlinear elastic base is a vital topic. It is beneficial for the design, manufacture, and practical application of these structures. This work is about to examine the nonlinear static response of a sandwich plate composed of a FG core and face sheets fabricated of piezoelectric material, where the whole plate is resting on a nonlinear elastic foundation. The FSDT and the finite element method are used to derive the finite element equations and the Newton–Raphson method is used to solve these equations.

The organization of this paper is divided into six main sections. Section 1 summarizes related works and gives the main reason for carrying out this investigation. Section 2 introduces the mathematical model of a piezoelectric sandwich FGM plate and its geometrical and material properties. Finite element modeling is clearly presented in Section 3. Accuracy examples are carried out in Section 4. Section 5 presents numerical results and discussions. Some important points of this work are drawn in Section 6.

2. Piezoelectric sandwich FGM plates resting on nonlinear elastic foundations

Consider an FGM sandwich consisting of five layers, where the innermost layer is made of ceramic, the outer two layers are made of FGM (the innermost layer and the outer two layers are called the core layer); the top and bottom face sheets are piezoelectric material as shown in Figure 1.

The material and structure of the plate are organized clearly in Figure 1. Herein, assuming that there is no delamination phenomenon among layers of the plate; c and m represent ceramic and metal, respectively. Ceramic and metal materials are distributed according to the simple power-law function. The volume fraction proportion of ceramic ($V_c^{(k)}$) and metal ($V_m^{(k)}$) of the kth layer (k = 1–3) is given by the following formula:

$$V_m^{(k)} + V_c^{(k)} = 1 \tag{1}$$

or in the clear form as follows:

$$\begin{cases} V_c^{(1)} = \left(\dfrac{2z+h}{h-h_1}\right)^n; & \dfrac{-h}{2} \le z \le \dfrac{-h_1}{2} \\ V_c^{(2)} = 1; & \dfrac{-h_1}{2} \le z \le \dfrac{h_1}{2} \\ V_c^{(3)} = \left(\dfrac{2z-h}{h_1-h}\right)^n; & \dfrac{h_1}{2} \le z \le \dfrac{h}{2}, \end{cases} \tag{2}$$

where h is the thickness of the sandwich plate, h_1 the thickness of the core layer, n the gradient index ($n \ge 0$), and z is the thickness coordinate variable.

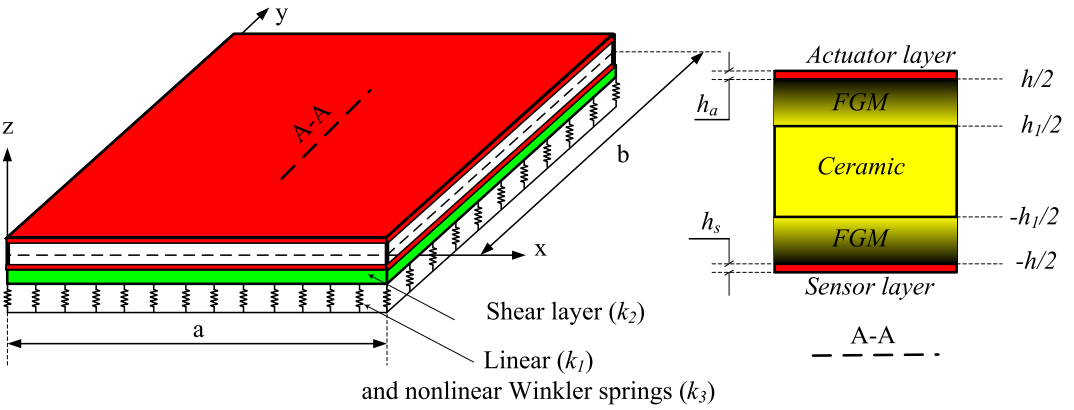

Figure 1. The geometry of a five-layered piezoelectric sandwich FGM plate resting on nonlinear elastic foundations.

The physical properties of the materials in each layer such as Young's modulus E, Poisson's ratio, etc., are dependent on the volume fraction proportion as:

$$\begin{Bmatrix} E^{(k)}(z) \\ \nu^{(k)}(z) \end{Bmatrix} = \begin{Bmatrix} E_m \\ \nu_m \end{Bmatrix} + \begin{Bmatrix} E_c - E_m \\ \nu_c - \nu_m \end{Bmatrix} V_c^{(k)}. \tag{3}$$

3. Finite element modeling of piezoelectric sandwich FGM plates

This paper uses the FSDT of Mindlin, the three-dimensional displacement field $(u^{(i)}, v^{(i)}, w^{(i)})$ of ith layer can be expressed in terms of five unknown variables as follows:

$$\begin{cases} u^{(i)} = u_0 + z^{(i)}\beta_x^{(i)} \\ v^{(i)} = v_0 + z^{(i)}\beta_y^{(i)} \\ w^{(i)} = w_0, \end{cases} \tag{4}$$

where u_0, v_0, and w_0 are the displacements along the x-, y-, and z-directions in the neutral plane of the plate; $\beta_x^{(i)}$ and $\beta_y^{(i)}$ are the transverse normal rotations of the y- and x-axes.

When considering the large deformation, the strain–displacement relations of ith layer is expressed as:

$$\begin{Bmatrix} \varepsilon_x \\ \varepsilon_y \\ \varepsilon_{xy} \\ \gamma_{xz} \\ \gamma_{yz} \end{Bmatrix}^{(i)} = \begin{Bmatrix} \dfrac{\partial u_0}{\partial x} + \dfrac{1}{2}\left(\dfrac{\partial w_0}{\partial x}\right)^2 + z^{(i)}\dfrac{\partial \beta_x^{(i)}}{\partial x} \\ \dfrac{\partial v_0}{\partial y} + \dfrac{1}{2}\left(\dfrac{\partial w_0}{\partial y}\right)^2 + z^{(i)}\dfrac{\partial \beta_y^{(i)}}{\partial y} \\ \dfrac{\partial u_0}{\partial y} + \dfrac{\partial v_0}{\partial x} + \dfrac{1}{2}\left(\dfrac{\partial w_0}{\partial x}\right)\left(\dfrac{\partial w_0}{\partial y}\right) + z^{(i)}\left(\dfrac{\partial \beta_x^{(i)}}{\partial y} + \dfrac{\partial \beta_y^{(i)}}{\partial x}\right) \\ \beta_x^{(i)} + \dfrac{\partial w^{(i)}}{\partial x} \\ \beta_y^{(i)} + \dfrac{\partial w^{(i)}}{\partial y} \end{Bmatrix}. \tag{5}$$

Equation (5) can be expanded in matrix form as follows:

$$\begin{Bmatrix} \boldsymbol{\varepsilon}^{(i)} \\ \boldsymbol{\gamma}^{(i)} \end{Bmatrix} = \begin{Bmatrix} \boldsymbol{\varepsilon}_m^{(i)} + \boldsymbol{\varepsilon}_N^{(i)} \\ \boldsymbol{\gamma}^{(i)} \end{Bmatrix} + \boldsymbol{z}^{(i)} \begin{Bmatrix} \boldsymbol{\kappa}^{(i)} \\ 0 \end{Bmatrix}, \tag{6}$$

where

$$\boldsymbol{\varepsilon}_m^{(i)} = \begin{Bmatrix} \dfrac{\partial u_0}{\partial x} \\ \dfrac{\partial v_0}{\partial y} \\ \dfrac{\partial u_0}{\partial y} + \dfrac{\partial v_0}{\partial x} \end{Bmatrix}; \quad \boldsymbol{\varepsilon}_N^{(i)} = \frac{1}{2} \begin{Bmatrix} \left(\dfrac{\partial w_0}{\partial x}\right)^2 \\ \left(\dfrac{\partial w_0}{\partial y}\right)^2 \\ \left(\dfrac{\partial w_0}{\partial x}\right)\left(\dfrac{\partial w_0}{\partial y}\right) \end{Bmatrix}; \quad \boldsymbol{\kappa}^{(i)} = \begin{Bmatrix} \dfrac{\partial \beta_x^{(i)}}{\partial x} \\ \dfrac{\partial \beta_y^{(i)}}{\partial y} \\ \dfrac{\partial \beta_x^{(i)}}{\partial y} + \dfrac{\partial \beta_y^{(i)}}{\partial x} \end{Bmatrix};$$

$$\boldsymbol{\gamma}^{(i)} = \begin{Bmatrix} \beta_x^{(i)} + \dfrac{\partial w^{(i)}}{\partial x} \\ \beta_y^{(i)} + \dfrac{\partial w^{(i)}}{\partial y} \end{Bmatrix}, \tag{7}$$

where $\boldsymbol{\varepsilon}_m^{(i)}$, $\boldsymbol{\kappa}^{(i)}$, $\boldsymbol{\gamma}^{(i)}$ are the membrane strain vector, curve vector, and shear strain vector, respectively. They are calculated from the displacements and the transverse normal rotations of the y- and x-axes.

Based on Hooke's law, the stress–strain relation in the case of piezoelectric effect taken into account is expressed as follows:

$$\begin{cases} \boldsymbol{\sigma}^{(i)} = \boldsymbol{D}_m^{(i)}(\boldsymbol{\varepsilon}_m^{(i)} + \boldsymbol{\varepsilon}_N^{(i)} + z^{(i)}\boldsymbol{\kappa}^{(i)}) - (\boldsymbol{e}^{(i)})^T \boldsymbol{E}_v^{(i)} \\ \boldsymbol{\tau}^{(i)} = \boldsymbol{D}_s^{(i)}\boldsymbol{\gamma}^{(i)} \\ \boldsymbol{D}^{(i)} = \boldsymbol{e}^{(i)}(\boldsymbol{\varepsilon}_m^{(i)} + z^{(i)}\boldsymbol{\kappa}^{(i)}) + \boldsymbol{p}^{(i)}\boldsymbol{E}_v^{(i)} \end{cases} \tag{8}$$

with

$$\boldsymbol{\sigma}^{(i)}(z) = \left[\sigma_x^{(i)} \ \sigma_y^{(i)} \ \sigma_{xy}^{(i)}\right]^T; \quad \boldsymbol{\tau}^{(i)}(z) = \left[\tau_{yz}^{(i)}(z) \ \tau_{xz}^{(i)}(z)\right]^T \tag{9a}$$

$$\boldsymbol{D}_m^{(i)}(z) = \frac{E^{(i)}(z)}{1-(\nu^{(i)}(z))^2} \begin{bmatrix} 1 & \nu^{(i)}(z) & 0 \\ \nu^{(i)}(z) & 1 & 0 \\ 0 & 0 & (1-\nu^{(i)}(z))/2 \end{bmatrix} \tag{9b}$$

$$\boldsymbol{D}_s^{(i)}(z) = \eta_c \cdot \frac{E^{(i)}(z)}{2(1+\nu^{(i)}(z))} \begin{bmatrix} 1 & 0 \\ 0 & 1 \end{bmatrix} \tag{9c}$$

where η_c is the shear correction factor and $\eta_c = 5/6$ is taken throughout the study.

• $\boldsymbol{E}_v$ is the electric field, which is determined through the variation of the potential as follows:

$$\boldsymbol{E}_v^{(i)} = -\nabla\phi^{(i)} = \begin{Bmatrix} 0 \\ 0 \\ E^{(i)z} \end{Bmatrix}. \tag{9d}$$

Herein, it is assumed that the electric field applies only to the plate in the thickness direction, and the symbol $E^{(i)z}$ is the electric field in the z-direction, which is calculated through the voltage and the thickness of the plate as follows:

$$E^{(i)z} = \frac{-\phi^{(i)}}{h_p}, \tag{9e}$$

where $h_p = h_a$ for actuator layer and $h_p = h_s$ for sensor layer.

• $\boldsymbol{D}^{(i)}$ is the electric displacement vector;

• $\boldsymbol{e}^{(i)}$ denotes the piezoelectric stress coefficients, which have the following precise expression [18]:

$$\boldsymbol{e}^{(i)} = \begin{bmatrix} 0 & 0 & 0 \\ 0 & 0 & 0 \\ e_{31}^{(i)} & e_{32}^{(i)} & 0 \end{bmatrix} \tag{9f}$$

• $\boldsymbol{p}^{(i)}$ is the dielectric tensor at constant mechanical strain with the expression as follows:

$$\boldsymbol{p}^{(i)} = \begin{bmatrix} p_{11}^{(i)} & 0 & 0 \\ 0 & p_{22}^{(i)} & 0 \\ 0 & 0 & p_{33}^{(i)} \end{bmatrix}. \tag{9g}$$

This paper uses a four-node plate element, each node has five DOF, and the displacement components at each node are expressed as follows:

$$\boldsymbol{q}_{2e} = \{u_{0j}\, v_{0j}\, w_j \beta_{xj} \beta_{yj}\}^T \quad \text{with } j = 1\text{–}4 \tag{10}$$

in which, the field variables, the independent displacement components at the reference plane may be expressed as follows:

$$\left[u_0, v_0, w_0, \beta_x, \beta_y\right]^T = \left[\sum_{j=1}^{4} N_j u_{0j}, \sum_{j=1}^{4} N_j v_{0j}, \sum_{j=1}^{4} N_j w_{0j}, \sum_{j=1}^{4} N_j \beta_{xj}, \sum_{j=1}^{4} N_j \beta_{yj}\right]^T, \tag{11}$$

where N_j is the Lagrangian interpolation function.

The displacements of one point in the neutral plane of the plate are interpolated through the shape functions and nodal displacement vector as:

$$\boldsymbol{v}_0 = \boldsymbol{N}\boldsymbol{q}_e \tag{12}$$

with

$$\boldsymbol{v}_0 = \left[u_0 \;\; v_0 \;\; w \;\; \beta_x \;\; \beta_y\right]^T \tag{13a}$$

$$\boldsymbol{q}_e = \left[\boldsymbol{q}_{1e} \;\; \boldsymbol{q}_{2e} \;\; \boldsymbol{q}_{3e} \;\; \boldsymbol{q}_{4e}\right]^T \tag{13b}$$

$$\boldsymbol{N} = \left[\boldsymbol{N}_1 \;\; \boldsymbol{N}_2 \;\; \boldsymbol{N}_3 \;\; \boldsymbol{N}_4\right], \tag{13c}$$

where $\boldsymbol{N}$ and $\boldsymbol{q}_e$ are the shape function matrix and the nodal displacement vector, respectively.

The strain vector components are now deployed according to the nodal displacement vector as follows:

$$\boldsymbol{\varepsilon}^{(i)} = (\boldsymbol{B}_1 + \boldsymbol{B}_N + \boldsymbol{B}_2)\boldsymbol{q}_e; \quad \boldsymbol{\gamma}^{(i)} = \boldsymbol{B}_3 \boldsymbol{q}_e \tag{14}$$

with

$$\boldsymbol{B_1} = \sum_{j=1}^{4} \begin{bmatrix} N_{j,x} & 0 & 0\;0\;0 \\ 0 & N_{j,y} & 0\;0\;0 \\ N_{j,y} & N_{j,x} & 0\;0\;0 \end{bmatrix}; \quad \boldsymbol{B_N} = \frac{1}{2}\sum_{j=1}^{4} \begin{bmatrix} \dfrac{\partial N_j}{\partial x} w_j & 0 \\ 0 & \dfrac{\partial N_j}{\partial y} w_j \\ \dfrac{\partial N_j}{\partial y} w_j & \dfrac{\partial N_j}{\partial x} w_j \end{bmatrix} \begin{bmatrix} 0\;0 & \dfrac{\partial N_j}{\partial x} & 0\;0 \\ 0\;0 & \dfrac{\partial N_j}{\partial y} & 0\;0 \end{bmatrix};$$

$$\boldsymbol{B_2} = \sum_{j=1}^{4} \begin{bmatrix} 0\;0\;0 & N_{j,x} & 0 \\ 0\;0\;0 & 0 & N_{j,y} \\ 0\;0\;0 & N_{j,y} & N_{j,x} \end{bmatrix}; \quad \boldsymbol{B_3} = \sum_{j=1}^{4} \begin{bmatrix} 0\;0 & N_{j,y} & 0 & N_j \\ 0\;0 & N_{j,x} & N_j & 0 \end{bmatrix}. \tag{15}$$

At this point, the electric field vector of the actuator layer and the sensor layer is expressed as follows:

$$\boldsymbol{E}_v = -\begin{bmatrix} 0, 0, \dfrac{1}{h_a} \\ 0, 0, \dfrac{1}{h_s} \end{bmatrix}^T \begin{Bmatrix} \phi_a \\ \phi_s \end{Bmatrix} = -\begin{bmatrix} \boldsymbol{B}_\phi^a \\ \boldsymbol{B}_\phi^s \end{bmatrix}^T \begin{Bmatrix} \phi_a \\ \phi_s \end{Bmatrix}, \tag{16}$$

where

$$\boldsymbol{B}_\phi^a = \left[0, 0, \frac{1}{h_a}\right]^T; \quad \boldsymbol{B}_\phi^s = \left[0, 0, \frac{1}{h_s}\right]^T \tag{17}$$

in which, h_a and h_s are the thicknesses of the actuator layer and sensor layer, respectively.

By integrating according to the plate thickness, normal forces, bending moments, and shear forces are obtained as follows:

$$\tilde{\boldsymbol{N}} = \begin{Bmatrix} \tilde{\boldsymbol{N}}_x \\ \tilde{\boldsymbol{N}}_y \\ \tilde{\boldsymbol{N}}_{xy} \end{Bmatrix} = \sum_{i=1}^{m} \int_{h_i}^{h_{i+1}} \begin{Bmatrix} \boldsymbol{\sigma}_x^{(i)}(z) \\ \boldsymbol{\sigma}_y^{(i)}(z) \\ \boldsymbol{\sigma}_{xy}^{(i)}(z) \end{Bmatrix} \mathrm{d}z = \sum_{i=1}^{m} \int_{h_i}^{h_{i+1}} \boldsymbol{D}_m^{(i)}(z) \cdot (\boldsymbol{\varepsilon}_m^{(i)} + \boldsymbol{\varepsilon}_N^{(i)} + z\boldsymbol{\kappa}^{(i)}) \, \mathrm{d}z \tag{18a}$$

$$\tilde{\boldsymbol{M}} = \begin{Bmatrix} \tilde{\boldsymbol{M}}_x \\ \tilde{\boldsymbol{M}}_y \\ \tilde{\boldsymbol{M}}_{xy} \end{Bmatrix} = \sum_{i=1}^{m} \int_{h_i}^{h_{i+1}} \begin{Bmatrix} \boldsymbol{\sigma}_x^{(i)}(z) \\ \boldsymbol{\sigma}_y^{(i)}(z) \\ \boldsymbol{\sigma}_{xy}^{(i)}(z) \end{Bmatrix} z \, \mathrm{d}z = \sum_{i=1}^{m} \int_{h_i}^{h_{i+1}} \boldsymbol{D}_m^{(i)}(z) (\boldsymbol{\varepsilon}_m^{(i)} + \boldsymbol{\varepsilon}_N^{(i)} + z\boldsymbol{\kappa}^{(i)}) z \, \mathrm{d}z \tag{18b}$$

$$\tilde{\boldsymbol{Q}} = \begin{Bmatrix} \tilde{\boldsymbol{Q}}_y \\ \tilde{\boldsymbol{Q}}_x \end{Bmatrix} = \sum_{i=1}^{m} \int_{h_i}^{h_{i+1}} \begin{Bmatrix} \boldsymbol{\tau}_{yz}^{(i)}(z) \\ \boldsymbol{\tau}_{xz}^{(i)}(z) \end{Bmatrix} \mathrm{d}z = \sum_{i=1}^{m} \int_{h_i}^{h_{i+1}} \boldsymbol{D}_s^{(i)}(z) \cdot \boldsymbol{\gamma}^{(i)} \, \mathrm{d}z. \tag{18c}$$

Equation (18) can be rewritten in matrix form

$$\begin{Bmatrix} \tilde{\boldsymbol{N}} \\ \tilde{\boldsymbol{M}} \\ \tilde{\boldsymbol{Q}} \end{Bmatrix} = \begin{bmatrix} \boldsymbol{A} & \boldsymbol{B} & \boldsymbol{0} \\ \boldsymbol{B} & \boldsymbol{D} & \boldsymbol{0} \\ \boldsymbol{0} & \boldsymbol{0} & \hat{\boldsymbol{A}} \end{bmatrix} \begin{Bmatrix} \boldsymbol{\varepsilon}_m + \boldsymbol{\varepsilon}_N \\ \boldsymbol{\kappa} \\ \boldsymbol{\gamma} \end{Bmatrix}, \tag{19}$$

where

$$(\boldsymbol{A}, \boldsymbol{B}, \boldsymbol{D}) = \sum_{i=1}^{m} \int_{h_i}^{h_{i+1}} (1, z, z^2) \boldsymbol{D}_m^{(i)}(z) \, \mathrm{d}z; \quad \hat{\boldsymbol{A}} = \sum_{i=1}^{m} \int_{h_i}^{h_{i+1}} \boldsymbol{D}_s^{(i)}(z) \, \mathrm{d}z. \tag{20}$$

The potential energy of the piezoelectric FGM plate in the case of taking into account the effect of the elastic foundation is given by the following formula:

$$\begin{aligned}
\delta \prod_e = & \int_{V_e} \begin{pmatrix} \delta \left\{ \boldsymbol{\varepsilon}_m^{(i)} + \boldsymbol{\varepsilon}_N^{(i)}, \boldsymbol{\kappa}^{(i)} \right\}^T \boldsymbol{\sigma}^{(i)} + \delta \boldsymbol{\gamma}^{(i)} \boldsymbol{\tau}^{(i)} - \delta (\boldsymbol{D}^{(i)})^T \boldsymbol{E}_v^{(i)} \\ k_1 \delta w w + k_2 \left(\delta \left(\dfrac{\partial w}{\partial x} \right) \left(\dfrac{\partial w}{\partial x} \right) + \delta \left(\dfrac{\partial w}{\partial y} \right) \left(\dfrac{\partial w}{\partial y} \right) \right) + k_3 \delta w w^3 \end{pmatrix} \mathrm{d}V \\
& - \int_{S_e} \delta \boldsymbol{v}^T \hat{\boldsymbol{F}} \, \mathrm{d}S - \int_{V_e} \delta \boldsymbol{E}_v^T \overline{\boldsymbol{Q}} \, \mathrm{d}V \\
= \delta \boldsymbol{q}_e^T & \int_{S_e} \begin{pmatrix} \boldsymbol{B}_1^T \boldsymbol{A} \boldsymbol{B}_1 + \boldsymbol{B}_1^T \boldsymbol{B} \boldsymbol{B}_2 + \boldsymbol{B}_2^T \boldsymbol{B} \boldsymbol{B}_1 + \boldsymbol{B}_2^T \boldsymbol{D} \boldsymbol{B}_2 + \boldsymbol{B}_3^T \hat{\boldsymbol{A}} \boldsymbol{B}_3 \\ \quad + \boldsymbol{B}_1^T \boldsymbol{A} \boldsymbol{B}_N + \boldsymbol{B}_N^T \boldsymbol{A} \boldsymbol{B}_1 + \boldsymbol{B}_2^T \boldsymbol{B} \boldsymbol{B}_N + \boldsymbol{B}_N^T \boldsymbol{B} \boldsymbol{B}_2 + \boldsymbol{B}_N^T \boldsymbol{A} \boldsymbol{B}_N \\ \quad + k_1 \boldsymbol{N}_w^T \boldsymbol{N}_w + k_2 \left(\left(\dfrac{\partial \boldsymbol{N}_w}{\partial x} \right)^T \left(\dfrac{\partial \boldsymbol{N}_w}{\partial x} \right) + \left(\dfrac{\partial \boldsymbol{N}_w}{\partial y} \right)^T \left(\dfrac{\partial \boldsymbol{N}_w}{\partial y} \right) \right) \\ \quad + k_3 \boldsymbol{N}_w^T \left(\sum_{j=1}^{4} N_j w_j \right)^2 \boldsymbol{N}_w \end{pmatrix} \mathrm{d}S \boldsymbol{q}_e \\
& - \delta \boldsymbol{q}_e^T \left(\int_{S_e} (-\boldsymbol{B}_1^T \boldsymbol{A} \boldsymbol{e}^T \boldsymbol{B}_{\phi a} - \boldsymbol{B}_2^T \boldsymbol{B} \boldsymbol{e}^T \boldsymbol{B}_{\phi a}) \, \mathrm{d}S \right) \phi_{ea} \\
& - \delta \boldsymbol{q}_e^T \left(\int_{S_e} (-\boldsymbol{B}_1^T \boldsymbol{A} \boldsymbol{e}^T \boldsymbol{B}_{\phi s} - \boldsymbol{B}_2^T \boldsymbol{B} \boldsymbol{e}^T \boldsymbol{B}_{\phi s}) \, \mathrm{d}S \right) \phi_{es} \\
& - \delta \phi_{ea}^T \left(\int_{S_e} (-\boldsymbol{B}_{\phi a}^T \boldsymbol{e} \boldsymbol{A} \boldsymbol{B}_1 - \boldsymbol{B}_{\phi a}^T \boldsymbol{e} \boldsymbol{B} \boldsymbol{B}_2) \, \mathrm{d}S \right) \boldsymbol{q}_e \\
& - \delta \phi_{es}^T \left(\int_{S_e} (-\boldsymbol{B}_{\phi s}^T \boldsymbol{e} \boldsymbol{A} \boldsymbol{B}_1 - \boldsymbol{B}_{\phi s}^T \boldsymbol{e} \boldsymbol{B} \boldsymbol{B}_2) \, \mathrm{d}S \right) \boldsymbol{q}_e \\
& - \delta \phi_{ea}^T \left(\int_{S_e} \boldsymbol{B}_{\phi a}^T \boldsymbol{p} \boldsymbol{B}_{\phi a}^T \, \mathrm{d}S \right) \phi_{ea} - \delta \phi_{es}^T \left(\int_{S_e} \boldsymbol{B}_{\phi s}^T \boldsymbol{p} \boldsymbol{B}_{\phi s}^T \, \mathrm{d}S \right) \phi_{es} \\
& - \delta \boldsymbol{q}_e^T \int_{S_e} \boldsymbol{N}^T \hat{\boldsymbol{F}} \mathrm{d}S - \delta \phi_{ea}^T \int_{V_e} \boldsymbol{B}_\phi^a \boldsymbol{Q}^a \, \mathrm{d}V - \delta \phi_{es}^T \int_{V_e} \boldsymbol{B}_\phi^s \boldsymbol{Q}^s \, \mathrm{d}V
\end{aligned} \tag{21}$$

in which, k_1 is the Winkler foundation stiffness, k_2 is the shear layer stiffness, and k_3 is nonlinear stiffness of the hardening nonlinear elastic foundation [15]. This work takes into account the nonlinear coefficient of the elastic foundation k_3; this makes the elastic energy of the plate to add this component, and it depends on the nonlinear function of the displacement w, so the calculation is also more complicated than the linear elastic one. Besides, the response of the structure is also different from that in the case of omitting the nonlinearity of the elastic foundation.

$N_w = \sum_{j=1}^{4} [0,0,N_j,0,0]$ and $\hat{\boldsymbol{F}}$ is the surface loading, and (21) is expressed in matrix form as:

$$\delta \prod_e = \begin{pmatrix} \delta \boldsymbol{q}_e^T (\boldsymbol{K}_{uue} + \boldsymbol{K}_{uue}^N) \boldsymbol{q}_e + \delta \boldsymbol{q}_e^T \boldsymbol{K}_{u\phi e}^a \phi_{ae} + \delta \boldsymbol{q}_e^T \boldsymbol{K}_{u\phi e}^s \phi_{se} \\ + \delta \phi_{ae}^T \boldsymbol{K}_{\phi ue}^a \boldsymbol{q}_e + \delta \phi_{se}^T \boldsymbol{K}_{\phi ue}^s \boldsymbol{q}_e \\ - \delta \phi_{ae}^T \boldsymbol{K}_{\phi\phi e}^a \phi_{ae} - \delta \phi_{se}^T \boldsymbol{K}_{\phi\phi e}^s \phi_{se} \end{pmatrix} - \delta \boldsymbol{q}_e^T \hat{\boldsymbol{P}}_e - \delta \phi_{ae}^T \boldsymbol{F}_{qe}^a - \delta \phi_{se}^T \boldsymbol{F}_{qe}^s; \quad (22)$$

and the stiffness matrices are calculated as:

$$\boldsymbol{K}_{uue} = \int_{S_e} \left(\begin{array}{l} \boldsymbol{B}_1^T \boldsymbol{A} \boldsymbol{B}_1 + \boldsymbol{B}_1^T \boldsymbol{B} \boldsymbol{B}_2 + \boldsymbol{B}_2^T \boldsymbol{B} \boldsymbol{B}_1 + \boldsymbol{B}_2^T \boldsymbol{D} \boldsymbol{B}_2 + \boldsymbol{B}_3^T \hat{\boldsymbol{A}} \boldsymbol{B}_3 \\ \quad + k_1 \boldsymbol{N}_w^T \boldsymbol{N}_w + k_2 \left(\left(\dfrac{\partial \boldsymbol{N}_w}{\partial x} \right)^T \left(\dfrac{\partial \boldsymbol{N}_w}{\partial x} \right) + \left(\dfrac{\partial \boldsymbol{N}_w}{\partial y} \right)^T \left(\dfrac{\partial \boldsymbol{N}_w}{\partial y} \right) \right) \end{array} \right) \mathrm{d}S \quad (23)$$

$$\boldsymbol{K}_{uue}^N = \int_{S_e} \left(\begin{array}{l} \boldsymbol{B}_1^T \boldsymbol{A} \boldsymbol{B}_N + \boldsymbol{B}_N^T \boldsymbol{A} \boldsymbol{B}_1 + \boldsymbol{B}_2^T \boldsymbol{B} \boldsymbol{B}_N + \boldsymbol{B}_N^T \boldsymbol{B} \boldsymbol{B}_2 + \boldsymbol{B}_N^T \boldsymbol{A} \boldsymbol{B}_N \\ \quad + k_3 \boldsymbol{N}_w^T \left(\sum_{j=1}^{4} N_j w_j \right)^2 \boldsymbol{N}_w \end{array} \right) \mathrm{d}S \quad (24)$$

$$\boldsymbol{K}_{u\phi e}^a = \int_{S_e} (-\boldsymbol{B}_1^T \boldsymbol{A} \boldsymbol{e}^T \boldsymbol{B}_{\phi a} - \boldsymbol{B}_2^T \boldsymbol{B} \boldsymbol{e}^T \boldsymbol{B}_{\phi a}) \, \mathrm{d}S \quad (25)$$

$$\boldsymbol{K}_{u\phi e}^s = \int_{S_e} (-\boldsymbol{B}_1^T \boldsymbol{A} \boldsymbol{e}^T \boldsymbol{B}_{\phi s} - \boldsymbol{B}_2^T \boldsymbol{B} \boldsymbol{e}^T \boldsymbol{B}_{\phi s}) \, \mathrm{d}S \quad (26)$$

$$\boldsymbol{K}_{\phi ue}^a = \int_{S_e} (-\boldsymbol{B}_{\phi a}^T \boldsymbol{e} \boldsymbol{A} \boldsymbol{B}_1 - \boldsymbol{B}_{\phi a}^T \boldsymbol{e} \boldsymbol{B} \boldsymbol{B}_2) \, \mathrm{d}S \quad (27)$$

$$\boldsymbol{K}_{\phi ue}^s = \int_{S_e} (-\boldsymbol{B}_{\phi s}^T \boldsymbol{e} \boldsymbol{A} \boldsymbol{B}_1 - \boldsymbol{B}_{\phi s}^T \boldsymbol{e} \boldsymbol{B} \boldsymbol{B}_2) \, \mathrm{d}S \quad (28)$$

$$\boldsymbol{K}_{\phi\phi e}^a = \int_{S_e} \boldsymbol{B}_{\phi a}^T \boldsymbol{p} \boldsymbol{B}_{\phi a}^T \, \mathrm{d}S \quad (29)$$

$$\boldsymbol{K}_{\phi\phi e}^s = \int_{S_e} \boldsymbol{B}_{\phi s}^T \boldsymbol{p} \boldsymbol{B}_{\phi s}^T \, \mathrm{d}S \quad (30)$$

$$\hat{\boldsymbol{P}}_e = \int_{S_e} \boldsymbol{N}^T \hat{\boldsymbol{F}} \cdot \mathrm{d}S_e \quad (31)$$

$$\boldsymbol{F}_{qe}^a = \int_{S_e} \boldsymbol{B}_\phi^{aT} \boldsymbol{Q}^a \, \mathrm{d}S; \quad \boldsymbol{F}_{qe}^s = \int_{S_e} \boldsymbol{B}_\phi^{sT} \boldsymbol{Q}^s \, \mathrm{d}S \quad (32)$$

in which, $\boldsymbol{Q}^a$ and $\boldsymbol{Q}^s$ are the voltages acting on actuator and sensor layers.

For the static bending problem, by minimizing the potential energy (22) by variables, these equations are obtained as:

$$\begin{cases} (\boldsymbol{K}_{uue} + \boldsymbol{K}_{uue}^N) \boldsymbol{q}_e + \boldsymbol{K}_{u\phi e}^a \phi_{ae} + \boldsymbol{K}_{u\phi e}^s \phi_{se} = \hat{\boldsymbol{P}}_e \\ \boldsymbol{K}_{\phi ue}^a \boldsymbol{q}_e + \boldsymbol{K}_{\phi\phi e}^a \phi_{ae} = \boldsymbol{F}_{qe}^a \\ \boldsymbol{K}_{\phi ue}^s \boldsymbol{q}_e + \boldsymbol{K}_{\phi\phi e}^s \phi_{se} = \boldsymbol{F}_{qe}^s. \end{cases} \quad (33)$$

By extracting ϕ_{ae}, ϕ_{se} from the second expression of (33), then substituting them into the first expression of (33), the equation with only the displacement $\boldsymbol{q}_e$ is obtained as follows:

$$\left(\begin{array}{l} (\boldsymbol{K}_{uue} + \boldsymbol{K}_{uue}^N) + \boldsymbol{K}_{u\phi e}^a \boldsymbol{K}_{\phi\phi e}^{a-1} \boldsymbol{K}_{\phi ue}^a \\ \quad + \boldsymbol{K}_{u\phi e}^s \boldsymbol{K}_{\phi\phi e}^{s-1} \boldsymbol{K}_{\phi ue}^s \end{array} \right) \boldsymbol{q}_e = \hat{\boldsymbol{P}}_e + \boldsymbol{K}_{u\phi e}^s \boldsymbol{F}_{qe}^s + \boldsymbol{K}_{u\phi e}^a \boldsymbol{F}_{qe}^a. \quad (34)$$

For the whole structure, the static equilibrium equation has the following form:

$$\sum_e \begin{pmatrix} (\boldsymbol{K}_{uue} + \boldsymbol{K}^N_{uue}) + \boldsymbol{K}^a_{u\phi e}\boldsymbol{K}^{a-1}_{\phi\phi e}\boldsymbol{K}^a_{\phi ue} \\ + \boldsymbol{K}^s_{u\phi e}\boldsymbol{K}^{s-1}_{\phi\phi e}\boldsymbol{K}^s_{\phi ue} \end{pmatrix} \boldsymbol{q_e} = \sum_e \left(\hat{\boldsymbol{P}}_e + \boldsymbol{K}^s_{u\phi e}\boldsymbol{F}^s_{qe} + \boldsymbol{K}^a_{u\phi e}\boldsymbol{F}^a_{qe} \right). \tag{35}$$

Equation (35) contains the nonlinear matrices of the plate and the elastic foundation, therefore, the Newton–Raphson method is used to solve this equation.

Herein, all integrations in the stiffness matrix and nodal force vector use the common Gauss quadrature rule. Hence, to avoid the shear-locking effect, selective integration is employed, where the reduced integration tacking a single quadrature point is utilized to compute the shear strain energy, whereas the full Gauss integration employing quadrature points is used to compute the bending strain energy.

4. Accuracy study

This section carries out verification problems. For easy tracking of numerical results, in this work, S represents the simply supported edge, C represents the clamped edge, and F represents the free edge. Then, SSSS represents the fully simply supported plate, and CCCC represents the fully clamped plate. For more details, the DOF of boundary conditions are described as follows:

For the SSSS boundary condition:

$$v_0 = w = \beta_y = 0, \quad \text{at } x = 0, a \tag{36a}$$

$$u_0 = w = \beta_x = 0, \quad \text{at } y = 0, b. \tag{36b}$$

For the CCCC boundary condition:

$$u_0 = v_0 = w = \beta_x = \beta_y = 0, \quad \text{at } x = 0, a \quad \text{and} \quad y = 0, b. \tag{37}$$

4.1. *A piezoelectric FGM plate under uniform load*

Consider a piezoelectric FGM plate with material properties: Al_2O_3/Ti–6Al–4V, $E_c = 320.24$ GPa, $\nu_c = 0.26$, $E_m = 105.7$ GPa, $\nu_m = 0.2981$. The dimensions of the plate: $a = b = 0.4$ m, $h = 5$ mm, $h_a = h_s = 0.1$ mm. Two piezoelectric layers are made of G-1195N with $E_{pi} = 63$ GPa, Poisson's ratio 0.3, $d_{31} = d_{32} = 254 \times 10^{-12}$ m/V, $k_{33} = 15$ nF/m. The plate is free at one edge, and the other three edges are clamped, so in this case, is called CFFF. The uniformly distributed load of 100 N/m^2 is applied to the plate, and actuator voltages $V = 0$ and 40 V are considered. The deflections at $y = b/2$ obtained from this work and [18] are presented in Figures 2 and 3 with the note that the top surface of the plate is the metal Ti–6Al–4V, and the bottom one is the ceramic Al_2O_3. It can be seen clearly that the results are in good agreement.

4.2. *An FGM plate resting on an elastic foundation under uniform load*

In this section, the verification for the plate resting on an elastic foundation is carried out. Consider a square plate with the dimensions $a = b = 0.2$ m, $h = a/10$ and $a/200$. Material properties are Young's modulus $E_c = E_m = 320.24$ GPa, and Poisson's ratio 0.26. The boundary condition of the plate is SSSS, and the plate is under the uniformly distributed load q_0. Two non-dimensional parameters of the elastic foundation are calculated as follows:

$$\begin{cases} k_1^* = \dfrac{k_1 a^4}{D} \\ k_2^* = \dfrac{k_2 a^2}{D} \end{cases} \tag{38}$$

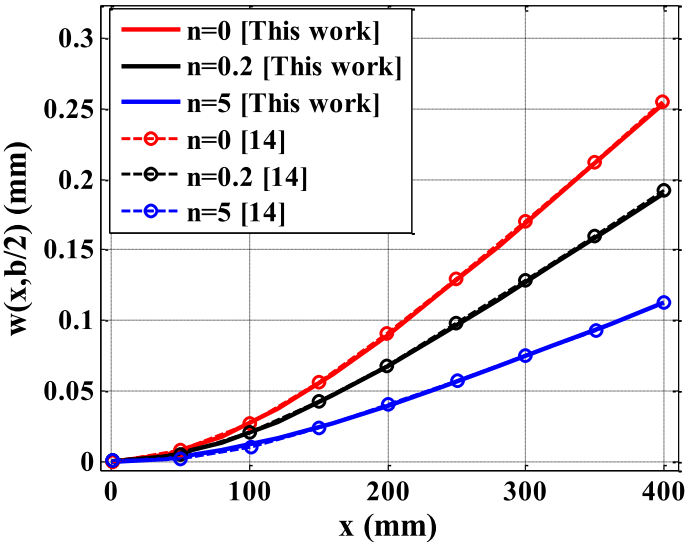

Figure 2. Deflection $w\,(x, y = b/2)$ of the FGM plate under a uniformly distributed load of 100 N/m^2 and actuator voltage $V = 0$ V.

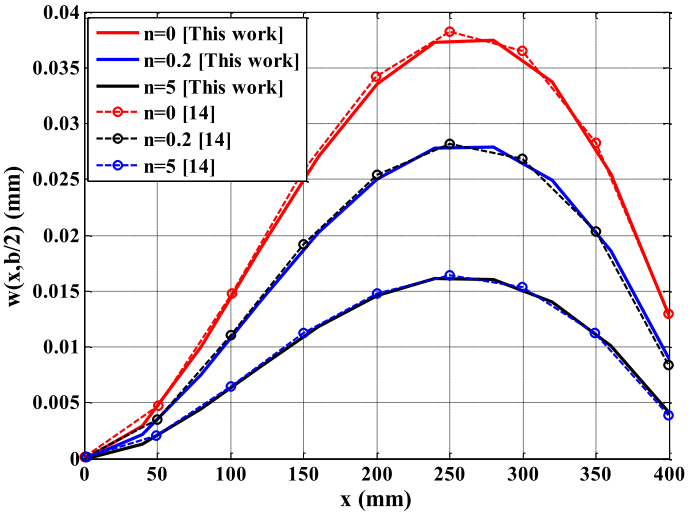

Figure 3. Deflection $w\,(x, y = b/2)$ of the FGM plate under a uniformly distributed load of 100 N/m^2 and actuator voltage $V = 40$ V.

with

$$D = \frac{E_c h^3}{12(1-\nu_c^2)}. \tag{39}$$

The non-dimensional deflection at the center point of the plate is defined by the following formula:

$$\overline{w} = \frac{10^3 D}{q_0 a^4} w\left(\frac{a}{2}, \frac{b}{2}\right). \tag{40}$$

The numerical results of this work are compared with those of the differential quadrature method [19] and the analytical method [20] as shown in Table 1.

Table 1. Comparative deflection $\overline{w}$ of the plate resting on the elastic foundation with different foundation parameters ($k_3^* = 0$)

k_1^*	k_2^*	$a/h = 10$				
		[19]	[20]	This work	Error with [19] %	Error with [20] %
1	5	3.3455	3.3455	3.3401	0.161	0.161
	10	2.7505	2.7504	2.7509	0.018	0.014
	15	2.3331	2.3331	2.3364	0.141	0.141
	20	2.0244	2.0244	2.0291	0.232	0.232
81	5	2.8422	2.8421	2.8448	0.095	0.091
	10	2.3983	2.3983	2.4034	0.212	0.212
	15	2.0730	2.0730	2.0792	0.299	0.299
	20	1.8245	1.8244	1.8311	0.367	0.361
625	5	1.3785	1.3785	1.3913	0.928	0.928
	10	1.2615	1.2615	1.2732	0.927	0.927
	15	1.1627	1.1627	1.1734	0.920	0.920
	20	1.0782	1.0782	1.0880	0.908	0.908

4.3. *Linear static bending of three-layered sandwich FGM plate under sinusoidally distributed load*

Next, the non-dimensional deflection and stress of the fully simply-supported sandwich (three layers) FGM plate are considered. The dimensions of the plate are $a/b = 1$, $a/h = 10$ (Figure 1); the core layer is ceramic ZrO_2 ($E_{ZrO_2} = 151$ GPa, $\nu_{ZrO_2} = 0.3$); two surface layers are FGM made from aluminum ($E_{Al} = 70$ GPa, $\nu_{Al} = 0.3$) and zirconium dioxide ZrO_2. If the thicknesses of two outer layers equal each other, and if the thickness of the outer layer is two times that of the core layer, it is represented as (2-1-2), similar meaning for (1-1-1) and other thickness ratios. The thickness ratio of three layers (2-1-2), (1-1-1), and (1-2-1) is used to compare in this subsection, respectively.

The plate is under the sinusoidally distributed load $q_0 = Q_0 \sin(\pi x/a)\sin(\pi y/b)$ with Q_0 representing the intensity of the load at the plate center. The numerical results are presented in Table 2, where Zenkour [21] used the analytical solution. It can be observed that the numerical results meet a good agreement. Moreover, readers will discover that since this study employs FSDT, the findings are comparable to those in [21], which uses FSDT theory. Furthermore, among the plate theories considered, the classical shear deformation theory (CLPT) consistently produces the lowest result.

Note that the non-dimensional deflection at the center point of the plate is normalized as:

$$\overline{w} = \frac{10hE_0}{Q_0 a^2} w_c\left(\frac{a}{2}, \frac{b}{2}\right), \tag{41}$$

where the reference value is taken as $E_0 = 1$ GPa.

4.4. *Nonlinear static bending of an FGM plate under uniform load*

Consider a fully-simply supported FGM plate under the uniformly distributed load q_0. The dimensions of the plate are $a = b$, plate thickness $h = a/100$. The material parameters of ceramic (c) and metal (m) are: $E_c = 151$ GPa, $\nu_c = 0.3$, $E_m = 70$ GPa, and $\nu_m = 0.3$. The normal nonlinear displacements (W_{max}/h) of the plate are solved by this work compared with Reddy's results [22] which are shown in Figure 4. We can see that the results obtained by this approach are in a good agreement with the reference results of Reddy [22].

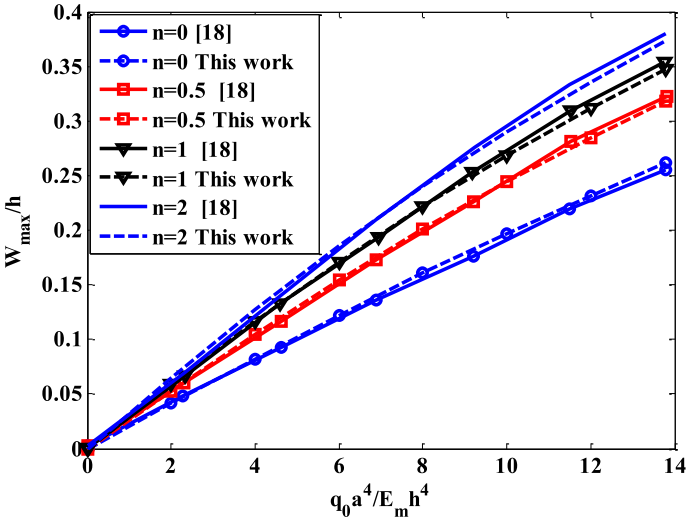

Figure 4. Comparison of non-dimensional nonlinear deflection of FGM plates.

Table 2. Comparison of $\overline{w}$ for a sandwich FGM plate with different values of volume fraction exponent n

n	Theory	$\overline{w}$		
		(2-1-2)	(1-1-1)	(1-2-1)
0	SSDPT [21]	0.1960	0.1965	0.1960
	TSDPT [21]	0.1960	0.1960	0.1960
	FSDT [21]	0.1960	0.1960	0.1960
	CLPT [21]	0.1856	0.1856	0.1856
	This work	0.1968	0.1968	0.1968
1	SSDPT [21]	0.3062	0.2919	0.2709
	TSDPT [21]	0.3063	0.2919	0.2709
	FSDT [21]	0.3075	0.2930	0.2716
	CLPT [21]	0.2941	0.2802	0.2595
	This work	0.3087	0.2940	0.2725
2	SSDPT [21]	0.3521	0.3328	0.3026
	TSDPT [21]	0.3523	0.3328	0.3026
	FSDT [21]	0.3540	0.3344	0.3037
	CLPT [21]	0.3394	0.3206	0.2909
	This work	0.3555	0.3356	0.3047
5	SSDPT [21]	0.3916	0.3712	0.3347
	TSDPT [21]	0.3918	0.3714	0.3348
	FSDT [21]	0.3941	0.3735	0.3363
	CLPT [21]	0.3778	0.3586	0.3228
	This work	0.3954	0.3750	0.3369
10	SSDPT [21]	0.4037	0.3849	0.3411
	TSDPT [21]	0.4040	0.2866	0.3482
	FSDT [21]	0.4065	0.3878	0.3499
	CLPT [21]	0.3894	0.3723	0.3361
	This work	0.4080	0.3891	0.3512

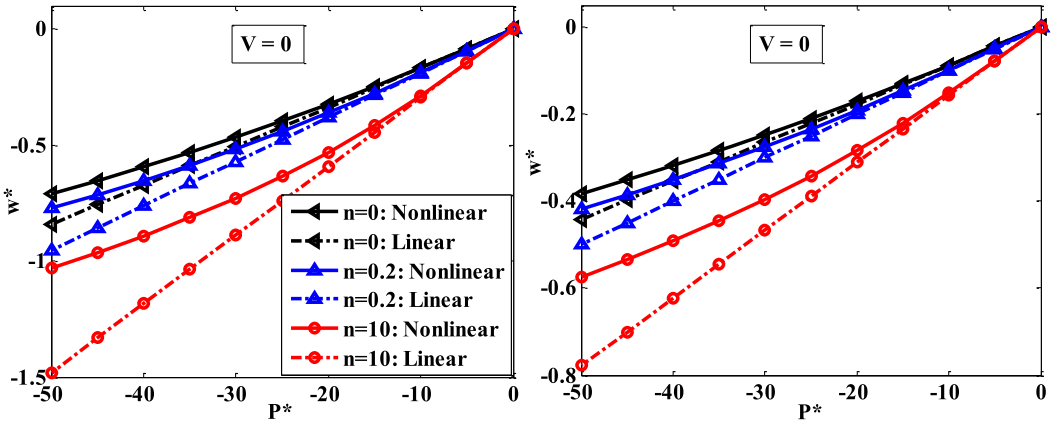

a. Location ($a/2$, $b/2$) b. Location ($a/4$, $b/4$)

Figure 5. The dependence of w^* on applied loads in the case of linear and nonlinear problems, $V = 0$.

Finally, through four verification problems, it can be concluded that the proposed theory and mathematical model used in this work ensures accuracy.

5. Numerical results and discussions

In this section, effects of some parameters on nonlinear static bending behaviors of piezoelectric sandwich FGM plates resting on nonlinear elastic foundations are investigated. The dimensions of the plate: $a = b = 0.4$ m, the plate thickness $h = a/100$. The core structure consists of three layers: the innermost layer is ceramic, the outer two layers are FGM. The characteristic parameters of ceramic and metal are: $E_c = 151$ GPa, $\nu_c = 0.3$, $E_m = 70$ GPa, and $\nu_m = 0.3$. For three layers of the sandwich FGM plate, as explained above, (2-1-2) represents the case of the thicknesses of two outer layers being equal, and two times more thick than the core layer.

The two surface layers are piezoelectric material G-1195N with $h_a = h_s = a/20$; material properties: $E_{pi} = 63$ GPa, Poisson's ratio $\nu_{pi} = 0.3$, $d_{31} = d_{32} = 254 \times 10^{-12}$ m/V, and $k_{33} = 15$ nF/m.

The plate is placed in the elastic foundation with the parameters k_1^*, k_2^*, which are defined as shown in (38) above, and coefficient k_3^* is defined as follows:

$$k_3^* = \frac{K_w a^6}{D}, \tag{42}$$

where D is expressed as presented in (39). The non-dimensional maximum deflection is calculated as $w^* = w/h$, where the calculated w value at two positions is ($a/2$, $b/2$) and ($a/4$, $b/4$); the plate is subjected to the uniformly distributed load P_0, and the non-dimensional load is $P^* = P_0 a^4/E_m h^4$.

5.1. *Effects of applied loads*

Consider a (2-1-2) FGM plate resting on the nonlinear elastic foundation with $k_1^* = 10$, $k_2^* = 1$, $k_3^* = 5$. By changing the voltage applied to the plate and increasing the mechanical load P_0, the dependencies of the non-dimensional maximum deflection w^* on the loads are shown in Figures 5–7. It can be seen that when increasing the mechanical load P_0, the deflection line in

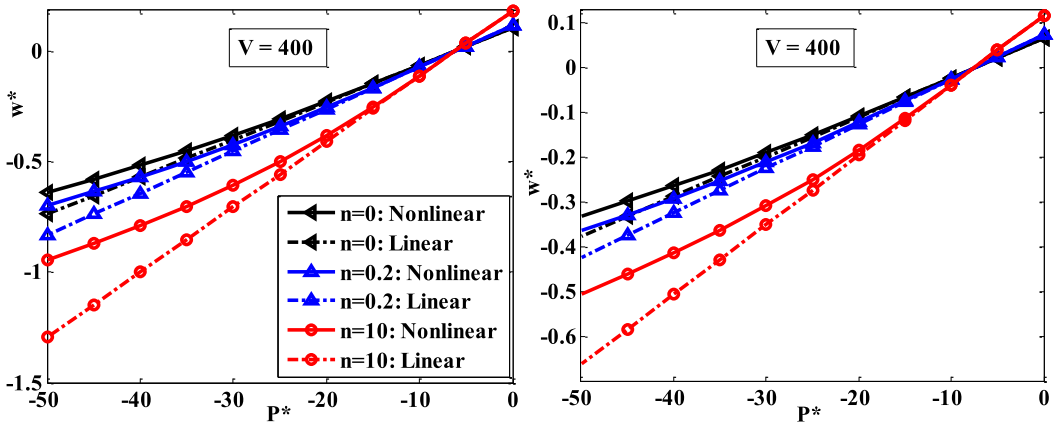

a. Location ($a/2$, $b/2$) b. Location ($a/4$, $b/4$)

Figure 6. The dependence of w^* on applied loads in the case of linear and nonlinear problems, $V = 400$.

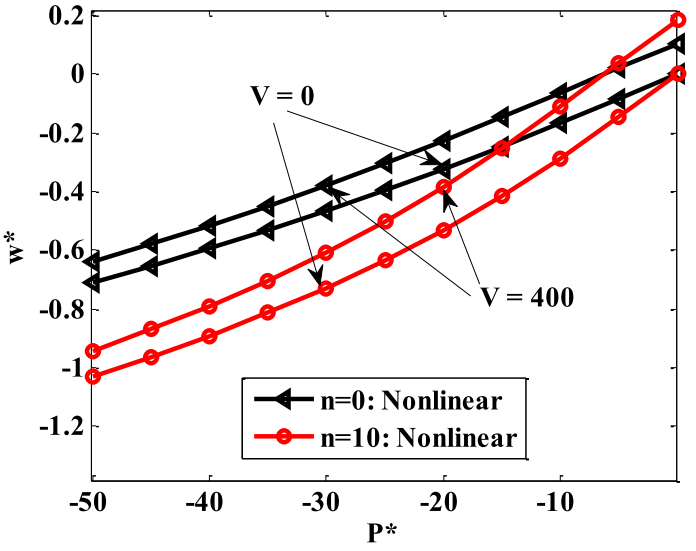

Figure 7. The dependence of w^* on applied loads in the case of linear and nonlinear problems, $V = 0$ and 400, location ($a/2$, $b/2$).

the case of the nonlinear problem is much different from that of the linear one. At the same time, increasing the voltage applied to the plate will reduce the non-dimensional maximum deflection w^*. This is the advantage of the FGM piezoelectric sandwich plate when setting a suitable voltage. Also, the reader can notice that the shape of the dependency of w^* on the load value P is the same at the two computation positions w, varying only in magnitude.

5.2. *Effects of elastic foundations*

Consider a (2-1-2) sandwich piezoelectric FGM plate resting on a nonlinear elastic foundation, where the foundation parameters (k_1^*, k_2^*, k_3^*) are varied in each investigation; and $n = 1$,

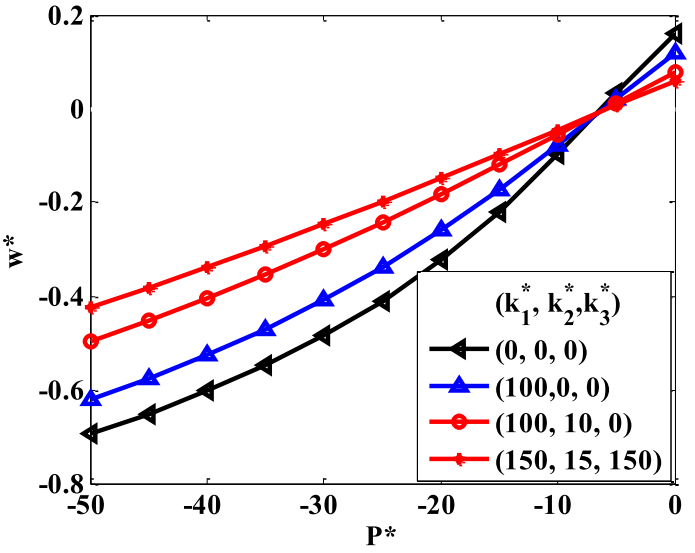

Figure 8. The dependence of w^* on $(k_1^*,\ k_2^*,\ k_3^*)$ with $n = 1$, $V = 400$ V, (2-1-2), location $(a/2, b/2)$.

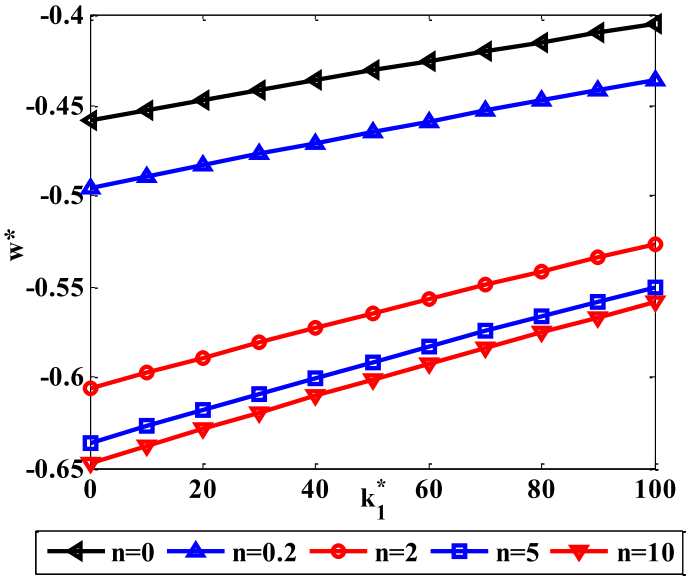

Figure 9. The dependence of w^* on k_1^* and n, with $V = 400$, $P^* = 40$, $k_2^* = 2$, $k_3^* = 2$, (2-1-2), location $(a/2, b/2)$.

$V = 400$ V. The dependence of non-dimensional maximum deflection w^* on the foundation parameters as well as the mechanical load P^* as shown in Figure 8. Figures 9 and 10 present the dependence of the non-dimensional maximum deflection w^* on the value of k_1^* and different values of volume fraction index n. In addition, Figure 11 presents the dependence of non-dimensional maximum deflection w^* on the value of k_1^* corresponding to different cases of the thickness ratio. From the numerical results, it can be seen that the higher the stiffness of the elastic foundation, the less obvious nonlinearity is. The deflection line of w^* depending on

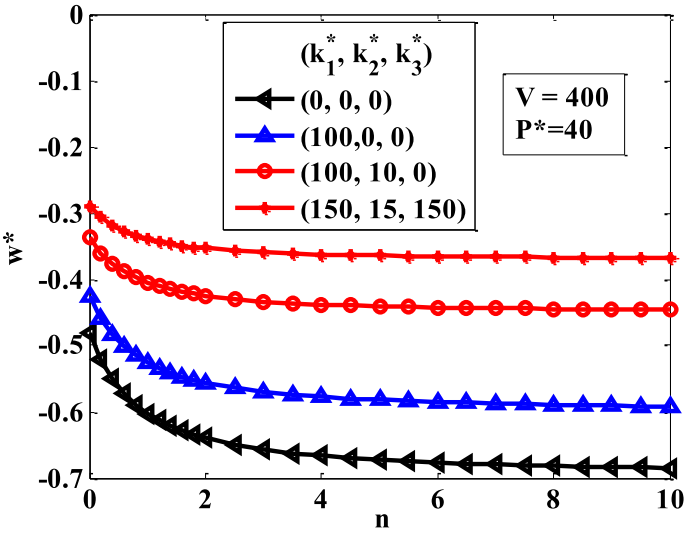

Figure 10. The dependence of w^* on (k_1^*, k_2^*, k_3^*) with $V = 400$, $P^* = 40$, (2-1-2), location $(a/2, b/2)$.

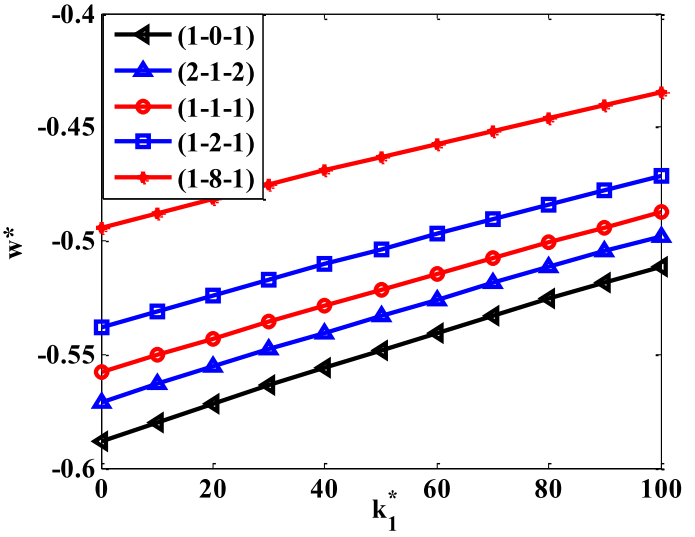

Figure 11. The dependence of w^* on k_1^* and the thickness ratio with $V = 400$, $P^* = 40$, $k_2^* = 2$, $k_3^* = 2$, location $(a/2, b/2)$.

the mechanical load is close to a linear line. When increasing the volume fraction index n, the proportion of metal is enhanced, the plate becomes softer, and the non-dimensional maximum deflection w^* increases; as n changes in a range of 0–2, the variation of w^* is strongest. When $n > 2$, the non-dimensional maximum deflection of w^* over n will change very slightly. The higher the thickness of the core layer, the larger the ceramic proportion of the plate, and as a result, the plate becomes stiffer, and the deflection of the structure reduces.

5.3. *Effects of boundary conditions*

To investigate the effect of boundary condition on the non-dimensional maximum deflection w^* of the plate, this section considers four types of boundary conditions such as SSSS, CFCF,

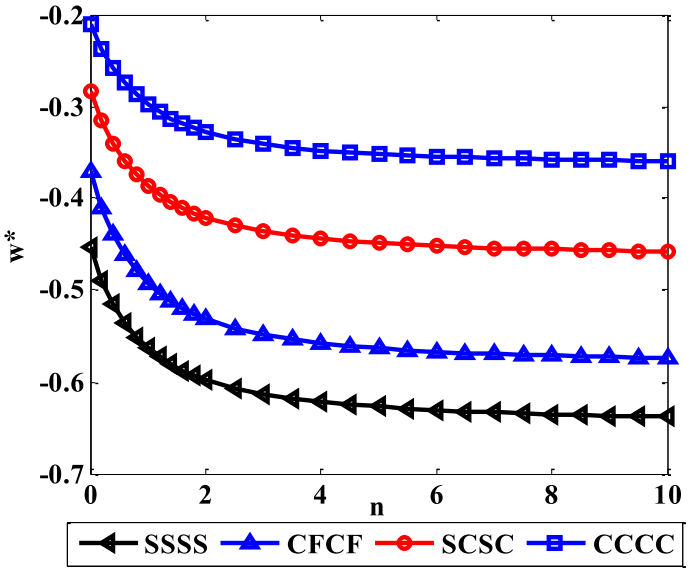

Figure 12. The dependence of w^* on boundary conditions and n, with $k_1^* = 10$, $k_2^* = 2$, $k_3^* = 2$, $V = 400$, $P^* = 40$, (2-1-2), location $(a/2, b/2)$.

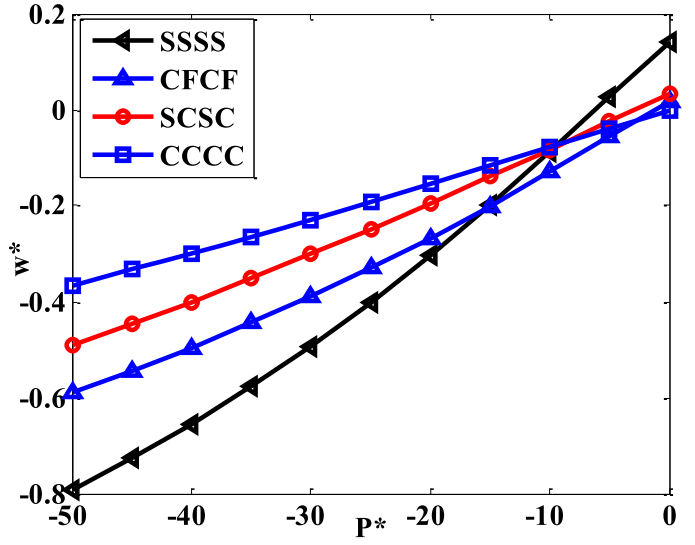

Figure 13. The dependence of w^* on boundary conditions and P^*, with $k_1^* = 10$, $k_2^* = 2$, $k_3^* = 2$, $V = 400$ V, $n = 1$, (2-1-2), location $(a/2, b/2)$.

SCSC, and CCCC. The dependence of w^* on the volume fraction index n, mechanical load P^*, and boundary conditions is shown in Figures 12–14. For the case of the SSSS plate, non-dimensional maximum deflection w^* has the highest value, and for the case of the CCCC plate, non-dimensional maximum deflection w^* has the smallest value. Besides, for the cases of the SSSS and CFCF plates, when increasing the value of P^*, the nonlinearity is more pronounced than that of the SCSC and CCCC cases. In final comment, increasing the value of the applied voltage, the non-dimensional maximum deflection w^* also reduces.

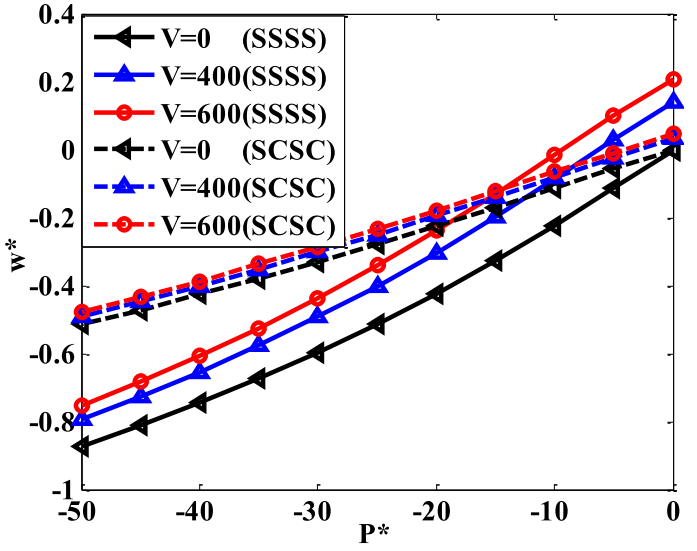

Figure 14. The dependence of w^* on boundary conditions and the applied voltage, with $k_1^* = 10$, $k_2^* = 2$, $k_3^* = 2$, $n = 1$, (2-1-2), location $(a/2, b/2)$.

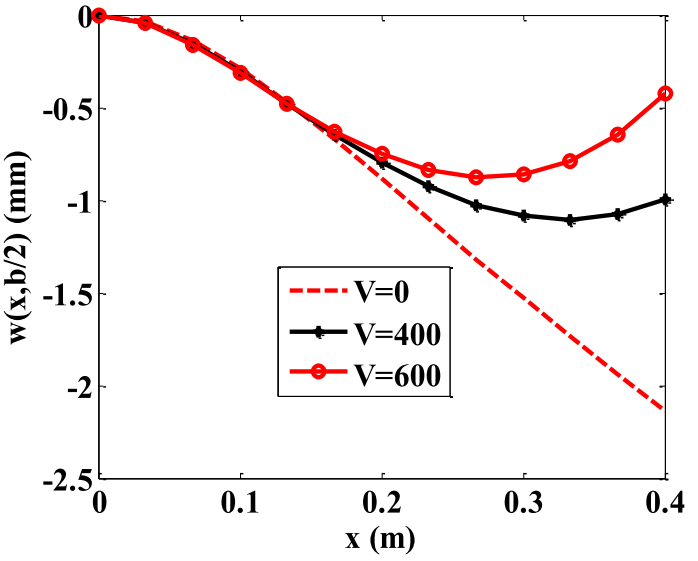

Figure 15. The dependence of $w\ (x, b/2)$ on V, with $k_1^* = 10$, $k_2^* = 2$, $k_3^* = 2$, $n = 1$, $P^* = 2$, (2-1-2).

5.4. *Deflections of CFFF plates*

Consider a CFFF plate, the deflection line w of the plate at $y = b/2$ with different values of the applied voltage is presented in Figure 15. Figure 16 presents the dependence of w on the volume fraction index n; the dependence of w on the parameter k_1^* is plotted in Figure 17. It can see that when there is no voltage applied to the plate, and the plate is only subjected to mechanical load, the point with the maximum displacement is located at $x = a = 0.4$ m. However, as the voltage V is applied to the plate, the maximum deflection point will move to the other point, and the

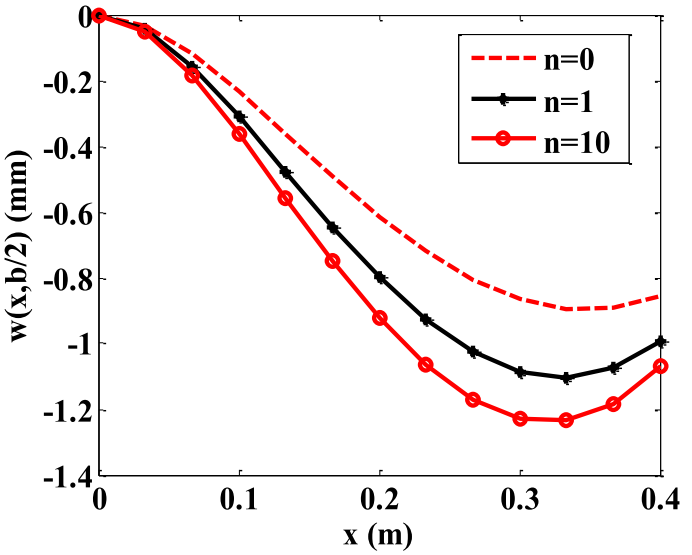

Figure 16. The dependence of $w\,(x, b/2)$ on n, with $k_1^* = 10$, $k_2^* = 2$, $k_3^* = 2$, $V = 400$, $P^* = 2$, (2-1-2).

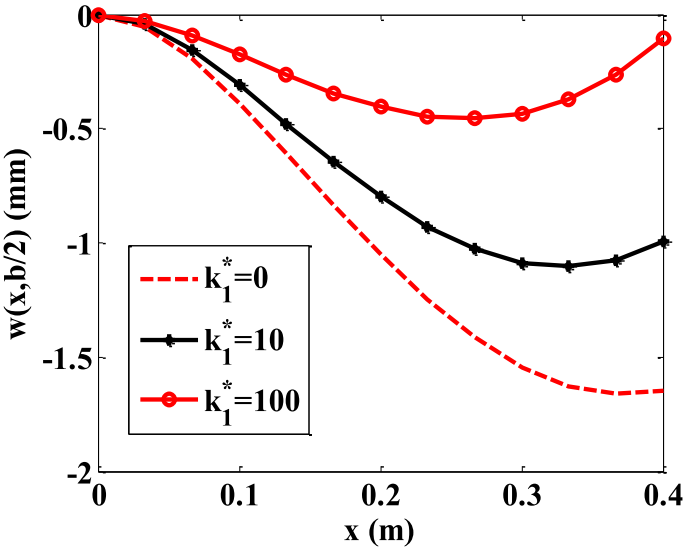

Figure 17. The dependence of $w\,(x, b/2)$ on k_1^*, with $k_2^* = 2$, $k_3^* = 2$, $V = 400$, $P^* = 2$, (2-1-2), $n = 1$.

shape of the deflection line at $y = b/2$ is also changed much. The increase of the applied voltage V also enhances the working capacity of the plate. The shape of the deflection line also changes as a function of the volume fraction index n as well as the stiffness parameter k_1^* of the elastic foundation.

6. Conclusions

For the first time, this paper employs the finite element method to investigate the nonlinear static bending response of piezoelectric FGM sandwich plates resting on elastic foundations taking into

account the nonlinear component. This is in stark contrast to previously published research. Simultaneously, the nonlinear response explored in this study will become more realistic for structures undergoing large deformations. The research findings have a substantial impact on the design, manufacture, and use of piezoelectric structures in real-world applications and engineering. Finite element formulations are based on the first-order shear deformation theory of Mindlin and the finite element method. Verification examples present the reliability of the proposed theory and mathematical model. Some main remarkable points can be concluded as follows:

- The difference between the linear and nonlinear factors is increased when the mechanical load increases. Therefore, the nonlinear results of this work are very meaningful.
- On increasing the applied voltage, the maximum deflection of the plate decreases for all cases of boundary conditions. The increase of the applied voltage V also enhances the working capacity of the plate, this is the important advantage of piezoelectric structures.
- For CFFF plates, when changing the values of the applied voltage, the volume fraction index, and the stiffness of the elastic foundation, both the value and the shape of the deflection are changed.
- When increasing the thickness of the core layer of the sandwich FGM plate as well as the stiffness of the elastic foundation, the maximum deflection of the plate reduces.

Data availability

Data used to support the findings of this study are included in the article.

Conflicts of interest

The author declares that there is no conflict of interest regarding the publication of this paper.

Acknowledgment

This work was supported by the University of Transport Technology Foundation for Science and Technology Development (grant number 1139/QD).

References

[1] J. S. Moita, A. L. Araújo, V. F. Correi, C. M. M. Soares, J. Herskovits, "Active-passive damping in functionally graded sandwich plate/shell structures", *Compos. Struct.* **202** (2018), p. 324-332.

[2] P. R. Saffari, M. Fakhraie, M. A. Roudbari, "Free vibration and transient response of heterogeneous piezoelectric sandwich annular plate using third-order shear deformation assumption", *J. Solid Mech.* **12** (2020), no. 2, p. 315-333.

[3] M. A. R. Loja, C. M. M. Soares, J. I. Barbosa, "Analysis of functionally graded sandwich plate structures with piezoelectric skins, using B-spline finite strip method", *Compos. Struct.* **96** (2013), p. 606-615.

[4] R. Moradi-Dastjerdi, A. Radhi, K. Behdinan, "Damped dynamic behavior of an advanced piezoelectric sandwich plate", *Compos. Struct.* **243** (2020), article no. 112243.

[5] A. Alibeigloo, "Coupled thermoelasticity analysis of FGM plate integrated with piezoelectric layers under thermal shock", *J. Therm. Stress.* **42** (2019), no. 11, p. 1357-1375.

[6] A. M. Zenkour, R. A. Alghanmi, "Hygro-thermo-electro-mechanical bending analysis of sandwich plates with FG core and piezoelectric faces", *Mech. Adv. Mater. Struct.* **28** (2021), no. 3, p. 282-294.

[7] V. Gorge, A. Benjeddou, R. Ohayon, "A sandwich finite element for the analysis of piezoelectric adaptive shells of revolution", *Rev. Eur. Élém. Finis* **11** (2002), no. 2–4, p. 217-231.

[8] S. Kapuria, S. D. Kulkarni, "Efficient finite element with physical and electric nodes for transient analysis of smart piezoelectric sandwich plates", *Acta Mech.* **214** (2010), no. 1–2, p. 123-131.

[9] S. B. Beheshti-Aval, M. Lezgy-Nazargah, "A coupled refined high-order global-local theory and finite element model for static electromechanical response of smart multilayered/sandwich beams", *Arch. Appl. Mech.* **82** (2012), no. 12, p. 1709-1752.
[10] T. S. Plagianakos, E. G. Papadopoulos, "Higher-order 2-D/3-D layer wise mechanics and finite elements for composite and sandwich composite plates with piezoelectric layers", *Aerosp. Sci. Technol.* **40** (2015), p. 150-163.
[11] H. D. Duc, V. D. Thom, X. N. Nguyen, V. V. Pham, T. T. Nguyen, "Multi-phase-field modelling of the elastic and buckling behaviour of laminates with ply cracks", *Appl. Math. Model.* **94** (2021), p. 68-86.
[12] A. M. Zenkour, R. A. Alghanmi, "Static response of sandwich plates with FG core and piezoelectric faces under thermo–electro–mechanical loads and resting on elastic foundations", *Thin-Walled Struct.* **157** (2020), article no. 107025.
[13] M. Mohammadimehr, A. Mohammadimehr, "Electro–elastic analysis of a sandwich thick plate considering FG core and composite piezoelectric layers on Pasternak foundation using TSDT", *Steel Compos. Struct.* **20** (2016), no. 3, p. 513-544.
[14] M. Abazid, M. Alotebi, M. Sobhy, "A novel shear and normal deformation theory for hygrothermal bending response of FGM sandwich plates on Pasternak elastic foundation", *Struct. Eng. Mech.* **67** (2018), no. 3, p. 219-232.
[15] H. Babaei, Y. Kiani, M. R. Eslami, "Thermomechanical nonlinear in-plane analysis of fix-ended FGM shallow arches on nonlinear elastic foundation using two-step perturbation technique", *Int. J. Mech. Mater. Design* **15** (2019), p. 225-244.
[16] V. T. Do, M. Z. Ashraf, H. D. Duc, "Buckling of cracked FG plate resting on elastic foundation considering the effect of delamination phenomenon", *Compos. Struct.* **273** (2021), article no. 114278.
[17] L. M. Thai, D. T. Luat, V. B. Phung, P. V. Minh, D. V. Thom, "Finite element modeling of mechanical behaviors of piezoelectric nanoplates with flexoelectric effects", *Arch. Appl. Mech.* **92** (2022), p. 163-182.
[18] X. Q. He, T. Y. Ng, S. Sivashanker, K. M. Liew, "Active control of FGM plates with integrated piezoelectric sensors and actuators", *Int. J. Solids Struct.* **38** (2001), p. 1641-1655.
[19] J. B. Han, K. M. Liew, "Numerical differential quadrature method for Reissner/Mindlin plates on two-parameter foundations", *Int. J. Mech. Sci.* **39** (1997), no. 9, p. 977-989.
[20] H. T. Thai, P. Minwo, D. H. Choi, "A simple refined theory for bending, buckling, and vibration of thick plates resting on elastic foundation", *Int. J. Mech. Sci.* **73** (2013), p. 40-52.
[21] A. M. Zenkour, "A comprehensive analysis of functionally graded sandwich plates. Part 1—Deflection and stress", *Int. J. Solids Struct.* **42** (2005), p. 5224-5242.
[22] J. N. Reddy, "Analysis of functionally graded plates", *Int. J. Numer. Methods Eng.* **47** (2000), p. 663-684.